AMERICAN ACADEMY™ OF OPHTHALMOLOGY

Correlation of Histologic Features with In Vivo Imaging of Reticular Pseudodrusen

Ursula Greferath, PhD,[1,*] *Robyn H. Guymer, PhD,*[2,3,*] *Kirstan A. Vessey, PhD,*[1] *Kate Brassington, PhD,*[2,3] *Erica L. Fletcher, PhD*[1]

Purpose: To determine the histologic and cellular correlates in the retina and retinal pigment epithelium (RPE) with the presence of optical coherence tomography-defined reticular pseudodrusen (RPD).

Design: Observation case using immunocytochemistry of an exenterated eye with immediate fixation after removal.

Participants: Two patients, one with confirmed RPD and the other with mid-peripheral drusen, underwent multimethod imaging before exenteration and immediate fixation of the posterior eyecup for high-resolution immunocytochemical analysis.

Methods: Optical coherence tomography (OCT) was compared with high-resolution immunocytochemistry using a range of cellular markers to determine changes in the RPE, photoreceptors, and gliosis.

Main Outcome Measures: Correlations of the appearance of reticular pseudodrusen on OCT and immunocytochemical analysis.

Results: Reticular pseudodrusen were deposits juxtaposed to photoreceptor outer segments extending through the outer nuclear layer and even beyond the outer limiting membrane. Deposits were rich in vitronectin, photoreceptor-associated proteins, and Iba1-immunoreactive immune cells. In contrast to conventional drusen the lipid stain Oil Red O failed to stain RPD. Cellular analysis revealed that RPD were associated with photoreceptor disruption and loss and localized gliosis. In addition, anomalies in the RPE were observed.

Conclusions: Reticular pseudodrusen represent subretinal deposits that extend through the outer nuclear layer, affect photoreceptor integrity, and are associated with retinal gliosis and RPE damage. *Ophthalmology 2016;123:1320-1331 © 2016 by the American Academy of Ophthalmology. This is an open access article under the CC BY-NC-ND license (http://creativecommons.org/licenses/by-nc-nd/4.0/).*

Supplemental video is available at www.aaojournal.org.

Drusen are a well-described biomarker of the early stages of age-related macular degeneration (AMD).[1] Reticular pseudodrusen (RPD) are a relatively recently described anomaly that have been associated with increasing risk of late AMD, especially geographic atrophy.[2–6] They commonly appear as discrete yellow-white dots scattered across the perifoveal region on color imaging and that have a characteristic target-like appearance on infrared imaging.[7] In addition, in some patients, RPD manifest as interconnected ribbons of material in the perifoveal region, or alternatively as small lesions scattered in more peripheral retinal regions.[7] Considerable debate remains about the nature of these lesions and their cause.

The cause of RPD remains controversial. Based on en face optical coherence tomography (OCT) and histopathologic analysis, RPD have been attributed to anatomic variations within the choroidal vasculature and loss of the middle choroidal layer in particular.[3,8–10] In contrast, dysfunction of the retinal pigment epithelium (RPE) has been attributed to the genesis of RPD because of the subretinal location of the deposits on spectral-domain (SD) OCT and the progression to geographic atrophy.[11,12]

Although a great deal has been learned in recent years using a range of imaging techniques,[13] few, if any, studies compare the histologic characteristics of retinae affected by RPD with real-time in vivo imaging. Moreover, most histopathologic studies performed to date have been limited to retinae collected after death with variable fixational artefacts (e.g., approximately 3 hours[14] and 2 hours 40 minutes[11]). The potential for postmortem artifacts to affect the interpretation of the histologic studies has led to a lack of consensus on the findings to date. A detailed analysis of the changes that occur in the retina and RPE is required to understand the possible causes of RPD and their significance for the progression of retinal pathologic features.

The central aim of this study was to characterize the histologic and cellular changes in the retina and RPE that correlate with the real-time appearance of RPD as determined on SD OCT. Our results show that in a human eye immediately fixed after exenteration, RPD are located within the outer nuclear layer and occur in regions where there are RPE disruption, localized photoreceptor anomalies, and localized retinal stress. In addition, using a range of

http://dx.doi.org/10.1016/j.ophtha.2016.02.009
ISSN 0161-6420/16

immunocytochemical markers, RPD were found to contain photoreceptor outer segment proteins and immune cells and lacked labeling for lipids. These results highlight the differences between RPD and conventional drusen and suggest that RPE dysfunction is associated with the presence of RPD.

Methods

Human Subjects and Tissue Collection

The macular research group at the Centre for Eye Research Australia and the Oculoplastic Unit at the Royal Victorian Eye and Ear Hospital have an ongoing collaboration to identify patients who require their eye to be removed as part of their cancer treatment. After identifying an eligible eye, the macular researchers approach the patient to request permission to examine their eye for research purposes after its removal. Eyes identified through this collaboration underwent laser treatment with a nanosecond laser because of our interest in determining the tissue response and method of action of these lasers; the results of that investigation have already been published.[15] Laser treatment was applied 5 days before exenteration. The first patient identified and approached to request permission for us to apply laser treatment to her eye in 2013 serendipitously had retinae with extensive RPD. In 2014, a second patient was identified who was matched in age to the first patient, but who did not have RPD, and underwent nanosecond laser treatment to her eye before exenteration and served as a control for the RPD eye. Retinal regions far removed from the lasered regions were evaluated in this study. All procedures and protocols adhered to the tenets of the Declaration of Helsinki and were approved by the Human Ethics Committee of the Royal Victorian Eye and Ear Hospital, Melbourne, Australia. Written informed consent was obtained from both patients after the nature and possible consequences of the study were explained.

Patient 1 was an 86-year-old white woman with a strong family history of AMD: both her parents and sister were diagnosed with AMD, although she had never been. Apart from asthma, she had no systemic illnesses. Her only medications were aspirin 100 mg daily and nonsteroidal inhalers for asthma. In September 2013, she was diagnosed with a high-grade, poorly differentiated right lower lid sebaceous cell carcinoma that required exenteration because she had undergone multiple previous resections of a lid tumor. Just before her operation, her best-corrected visual acuity was 20/30 in both eyes. On dilated fundus examination, she had widespread RPD throughout the macula and above the arcades in both retinae, seen clinically and confirmed on imaging. There were fewer than 10 small (<63 μm) drusen visible in either eye.

Patient 2 was an 86-year-old white woman with a history of rheumatic heart disease, hypertension, and hypercholesterolemia who underwent aortic valve replacement in 2002. She was in atrial fibrillation and was taking digoxin, warfarin, and aspirin (100 mg daily) as well as atorvastatin (40 mg daily) for hypercholesterolemia. Her ocular history included herpetic scarring of the right cornea and several operations on her right lower lid for chronic entropion and trichiasis since 2002. In 2014, she required an exenteration of her right eye for an aggressive sclerosing basal cell carcinoma of her right lower lid extending into her orbit, restricting her eye movements, and causing globe displacement and diplopia. Just before her operation, her best-corrected visual acuity was 20/80 in her right eye and 20/20 in her left eye. She had scattered intermediate drusen (63−125 μm) in both eyes in the mid periphery. There was no clinical evidence or imaging evidence of RPD.

Imaging and Image Analysis

Multimethod imaging was performed on patient 1 the day before the exenteration, after the pupil was dilated with tropicamide 0.5% (Mydriacyl; Alcon, Frenchs Forrest, Australia). Color fundus images were obtained using a nonmydriatic fundus camera (Canon CR6-45NM; Canon, Saitama, Japan) and near-infrared fundus autofluorescence, and SD OCT volume scans were obtained using a Spectralis HRA+OCT device (Heidelberg Engineering, Heidelberg, Germany). Scans were performed over the central 20°×20° area, with 49 equally spaced horizontal B-scans used. Each B-scan contained 1024 A-scans and was set to average 25 frames each. The grading of color fundus photographs was performed using OptomizePro (Digital Healthcare Image Management System; Digital Healthcare Ltd, Cambridge, United Kingdom). The presence of RPD also was determined by examination of the near-infrared fundus autofluorescence and SD OCT imaging by one of the authors (R.H.G.). Because of media opacity in patient 2, it was not possible to obtain high-quality images on SD OCT.

Genetics

DNA was isolated from venous blood leukocytes and 10 ng of genomic DNA was amplified using polymerase chain reaction analysis in a multiplex reaction using Hotstart Taq polymerase (Bioline, London, United Kingdom). A MassEXTEND reaction was undertaken using the designed primers, samples were spotted onto a 384 SpectroCHIP II microarray, and genotyping was performed on the MassArray platform (Sequenom, San Diego, CA). The samples were screened for haplotype-tagging single-nucleotide polymorphisms in complement factor H (*CFH*) (Y402H, rs1061170, and rs10737680), and *ARMS2* (rs10490924).[16]

Retinal Fixation and Immunocytochemistry

During surgery, immediately after exenteration, the eyes were handed to the research staff, who dissected the globe, removing the anterior contents of the eye. The posterior eyecups then were placed into a solution containing 4% paraformaldehyde in 0.1 M phosphate buffer (PB) for 4 hours. The time between exenteration and fixation was approximately 10 minutes. Eyecups then were rinsed in 0.1 M PB and photographed. With visualization through a dissecting microscope, eyecups were dissected into pieces (approximately 4 mm^2) with a scalpel blade, whereby the exact location and eccentricity were mapped. Pieces were cryoprotected in graded sucrose solutions (10%, 20%, 30% weight/volume), snap-frozen, and stored at −80° C. Pieces of interest were thawed and embedded in Tissue-Tek OCT Compound (Tissue Tek; Sakura Finetek, Tokyo, Japan), cryosectioned (14 μm sections), and collected on polysine glass adhesion slides (Thermo Scientific, Scoresby, Australia). Slides were stored at −80° C until required.

Immunocytochemical labeling was performed on cryostat sections using the indirect fluorescence method as described previously.[17] Briefly, after thawing and rinsing (3 × 10 minutes in 0.1 M PB), primary antisera, diluted in a buffer containing 3% normal goat serum, 1% bovine serum albumin (BSA), and 0.5% Triton X-100 in 0.1 M PB, were applied to sections overnight at room temperature. For retinal flat mounts, the retina was peeled off the RPE and incubated for 3 to 6 days free floating at 4° C. For RPE flat mounts, the choroid and attached RPE were removed carefully from the underlying sclera. The choroid—RPE sheets were incubated (free floating) for 3 nights at 4° C.

The primary antibodies that were used in this study included a marker of Müller cell change, rabbit anti−glial fibrillary acidic protein (GFAP; Dako, Carpinteria, CA; catalog no., Z0334; diluted 1:20,000), marker for either short-wavelength or medium- to

long-wavelength cone opsins (rabbit antihuman S or M/L opsins, 1:100,000; kind gifts from Dr. J. Nathans), marker for cones, peanut agglutinin-rhodamine (Vector Labs; catalog no., RL-1072; diluted 1:250), an antibody specific to the extracellular matrix glycoprotein vitronectin (mouse anti-vitronectin; Santa Cruz Biotechnology; catalog no., sc-74485; diluted 1:100), a marker for microglia and macrophages, rabbit anti-IbA1 (Wako Pure Chemical Industries, Richmond, VA; catalog no., 019-19741; diluted 1:1500), and a marker for RPE cell membranes, Alexa Fluor 633-Phalloidin (Life Technologies, Mulgrave, Australia; diluted 1:200). After incubation and rinsing in 0.1 M PB, the appropriate goat−antirabbit or goat−antimouse Alexa Fluor 488 or 594 secondary antibody (Life Technologies) was applied at 1:500 dilution together with the nuclear stain BisBenzimide H (0.1 mg/ml; Sigma Aldrich, Castle Hill, Australia; catalog no., 14530) for 1 hour. Slides then were rinsed in 0.1 M PB and cover slipped with mounting medium (Dako).

Retinal and RPE−choroid flat mounts were washed in PB and mounted on slides using fine brushes. Spacer rings (100 μm thick) made from rubber tubing were placed around the mounted retinal pieces to prevent squashing of the retinal photoreceptor inner segment−outer segment junctions. Flat mounts were cover slipped with mounting medium (Dako).

After dissection and mapping, some pieces of the posterior eyecups were postfixed overnight in a fixative containing glutaraldehyde (1% paraformaldehyde, 2.5% glutaraldehyde, 3% sucrose, and 0.01% calcium chloride in 0.1 M PB; pH 7.4), washed in 0.1 M PB, and then dehydrated in methanol (75%, 85%, 95%, in water and 100%) and acetone (100%). Tissues were embedded in Epon resin (ProSciTech, Townsville City, Australia) that was polymerized. Semithin sections were cut at 1 μm with a microtome (Ultracut S; Reichert, Depew, NY). Retinal sections were stained with 1% toluidine blue and imaged (Axioplan; Zeiss, Gottingen, Germany).

Histochemical Labeling of Lipid with Oil Red O

To label for esterified cholesterol and other lipids, retinal sections were labeled with the lipid marker Oil Red O (Sigma Aldrich). Briefly, cryostat sections were postfixed in 4% paraformaldehyde for 15 minutes, briefly rinsed in water, and rinsed in 60% isopropanol. They were the stained for 40 minutes in freshly prepared Oil Red O working solution (Oil Red O 0.3% in isopropanol; Sigma Aldrich). Then, they were washed in water and cover slipped in mounting medium.

Determination of Cell Death

Cell death was detected using a terminal deoxynucleotidyl transferase dUTP nick end labeling (TUNEL) detection kit (DeadEnd Flurometric TUNEL system no. TB235; Promega Corp., Auburn, Australia) as previously described.[18] Six vertical cryostat sections from the macula were examined. Retinal sections were washed in 0.85% sodium chloride for 5 minutes, rinsed in phosphate-buffered saline (PBS) for 5 minutes, and then incubated in 0.2% Triton-X-100 in 0.1 M PBS for 12 minutes. The retinal sections then were washed 3 times in PBS for 5 minutes and equilibrated using equilibration buffer (200 mM potassium cacodylate, pH 6.6; 25 mM Tris-hydrogen chloride (HCL); 0.2 mM dithiothreitol (DTT); 0.25 mg/ml BSA; and 2.5 mM cobalt chloride) for 10 minutes. Sections were covered in reaction mix (a solution containing equilibration buffer, nucleotide mix [50 μM fluorescence-12-dUTP, 100 μM dATP, 10 mM Tris-HCl, 1 mM acetic acid] and rTdT enzyme) for 1 hour at 37° C. The reaction was stopped with a buffer containing 0.3 M sodium chloride and 0.15 M sodium citrate at pH 7.2, and then the sections were rinsed 3 times in PBS for 5 minutes. After TUNEL labeling, cell nuclei were counterstained with a 32-μM solution of 7-aminoactinomycin-D and cover slipped in mounting medium (Dako).

Microscopy and 3-Dimensional Reconstruction

Vertical sections of immunolabeled retina were viewed on either a Meta or Pascal confocal microscope (Zeiss, Oberkochen, Germany) using ×20 air or ×40 oil objectives and with appropriate filters for differential visualization of the specific fluorophores. Images were collected using Zeiss LSM or Zen software (Carl Zeiss AG, Jena, Germany) and were edited using Zeiss LSM software. Confocal Z-series that spanned the layers of interest in flat-mounted retinae were acquired with the optimal pinhole size (1 Airy unit), as suggested by the software.

For 3-dimensional reconstruction, labeled flat-mounted pieces of retinae were imaged as Z-stacks and reconstructed using IMARIS software version 7.7.0 (×64; Bitplane AG, Zürich, Switzerland). Confocal Z-stacks were reconstructed into 3-dimensional images in the Surpass mode. Background noise of each fluorescent channel was minimized individually on the Display Adjustments panel. Images were cropped to the relevant part of the field without altering the resolution. Three-dimensional representations of photoreceptor outer and inner segments with intercalating RPDs in confocal Z-stacks were created with the Surface function. Rendered images of different magnifications were captured using the Snapshot function and exported as .tif files.

Thickness of the outer nuclear layer (ONL) was measured in regions immediately above the RPD and also in adjacent areas devoid of RPD using Zeiss LSM software. Vertical sections from the foveal retina that were labeled for vitronectin and DAPI were measured. Ten measurements were obtained over each vitronectin-positive RPD and adjacent vitronectin immune-negative region that extended from the outer limiting membrane to the distal edge of the outer plexiform layer. In total, quantification of 50 RPD and 50 adjacent regions were used to determine whether RPD were associated with a change in ONL thickness.

To measure retinal stress, GFAP immunolabeling of Müller cells was quantified in retinal regions overlying RPD compared with regions immediately adjacent.[19] Using Zeiss LSM software, the pixel intensity was measured in retinal regions overlying RPD and compared with regions immediately adjacent. Glial fibrillary acidic protein labeling intensity in the distal inner plexiform layer was measured in the retina overlying 50 RPD and 50 neighboring areas.

Statistics and Analysis

A 1-way analysis of variance was used to validate statistically the change in GFAP immunolabeling or ONL thickness in areas with RPD compared with regions without RPD. Correlation between RPD area and either ONL thickness or GFAP immunolabeling was performed using a Pearson correlation. Statistical analyses and graphs were produced using GraphPad Prism software (San Diego, CA).

Results

Reticular pseudodrusen of the "dot" variety were seen across the posterior pole on examination and color fundus photographs of patient 1 and confirmed on fundus autofluorescence and infrared imaging and SD OCT in the week before exenteration (Fig 1A−D).[7] Only a few small (63 μm) hard drusen were observed. The retinal fundus of patient 1 immediately after fixation is shown

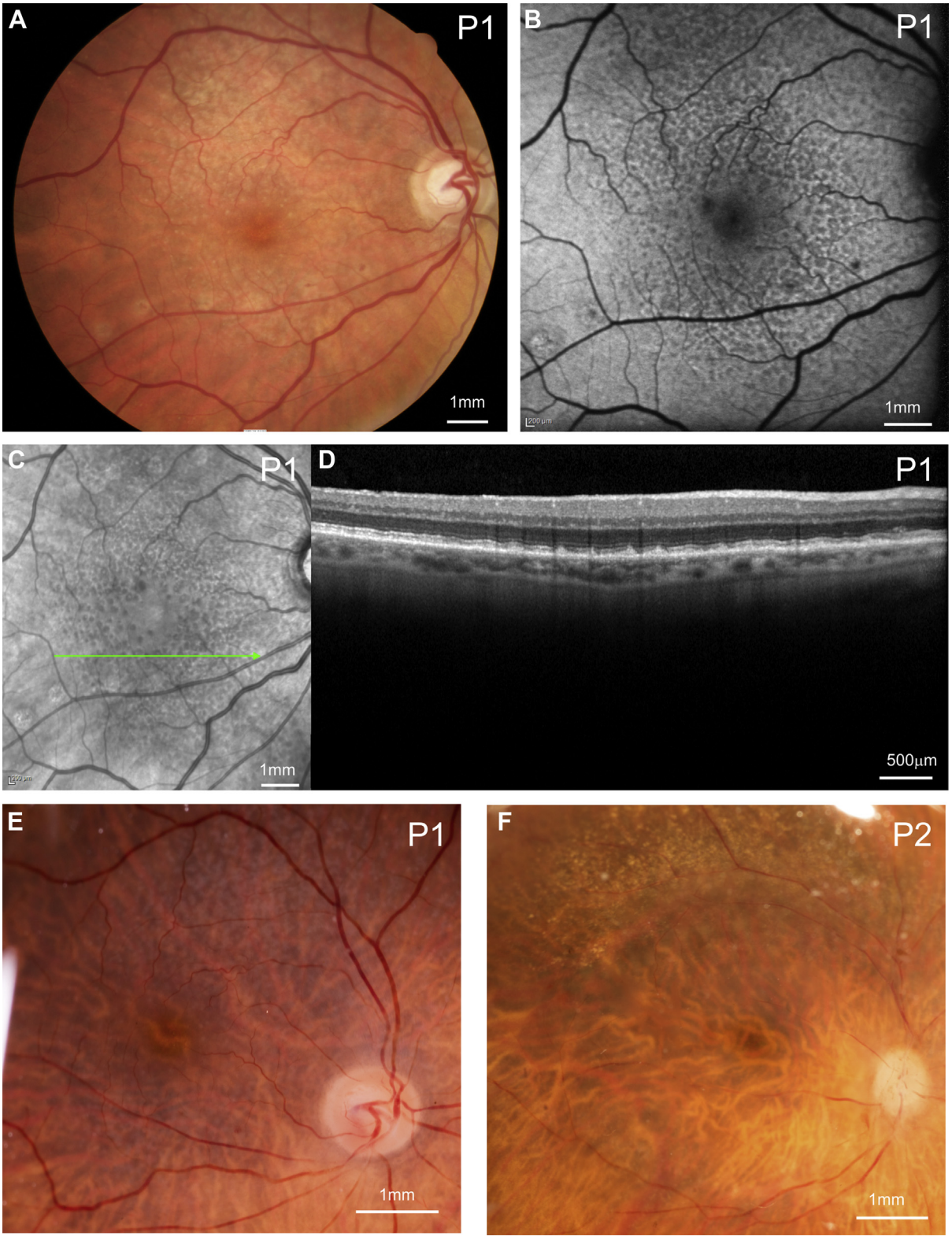

Figure 1. Fundus imaging. **A**, Color fundus photograph of the right eye of patient 1 (P1) before exenteration. Suprathreshold nanosecond laser spots are visible along the inferior arcade. **B**, Autofluorescent image showing characteristic reticular pseudodrusen (RPD). **C**, **D**, Red-free fundus image (**C**) and corresponding optical coherence tomography image (**D**) showing RPD visible as subretinal conical lesions. **E**, Color micrograph of the retinal fundus of P1 immediately after fixation. **F**, Color micrograph of the retinal fundus of patient 2 (P2) immediately after fixation. Subtle changes are seen along the superior arcade where the nanosecond laser was applied.

in Figure 1E. Patient 2 had intermediate drusen (63−125 μm) seen clinically in the mid periphery. No RPD were seen. Because of media opacity in patient 2, it was not possible to obtain high-quality images on SD OCT. However, an image of the retinal fundus immediately after fixation is shown in Figure 1F. Patient 1 was heterozygous for the complement factor H risk alleles (rs1061170; Y402H) and rs10737680, whereas patient 2 was heterozygous for rs1061170 but homozygous at risk for rs10737680. Patient 1 also was homozygous for the ARMS2 (rs104909240) risk allele, whereas patient 2 was homozygous protective for that allele.

To establish the location of RPD relative to the RPE, we first carefully aligned a region of retina that had been imaged with fundus imaging and had undergone histologic analysis. As shown in Figure 2, several characteristic RPD were visible in the SD OCT images as white triangular lesions projecting into the subretinal space (Fig 2A, small arrows; Fig 2B, black arrowheads). These lesions were identified in vertical histologic sections (Fig 2C). In particular, vitronectin stained RPD intensely and confirmed the subretinal location of these lesions and the penetration of debris through the outer limiting membrane into the ONL (Fig 2C, right-hand lesion) up to the outer plexiform layer. The location and appearance of the RPD when stained corresponded exactly to the in vivo SD OCT−imaged RPD lesions (Fig 2).

Reticular pseudodrusen have been classified into 3 stages depending on the level of distortion and visibility of the inner segment−ellipsoid band.[20] As shown in Figure 3, vitronectin immunolabeled a range of subretinal deposits from long, flat lesions (stage 1) to larger conical lesions that penetrated the outer limiting membrane into the ONL (Fig 3E, stage 2; Fig 3F, stage 3). In comparison, vitronectin also immunolabeled a small drusen in patient 2, but this was located beneath the RPE (Fig 3C).

We examined the effect that these deposits had on photoreceptor outer segments. Figure 4A shows an SD OCT image of an RPD, and Figure 4B shows a vertical section of the corresponding region through the same RPD, triple-labeled with the cone marker peanut agglutinin (red), vitronectin (green), and a nuclear counterstain (blue). The RPD deposit appears to have pushed the photoreceptor outer segments to the side. In addition, vitronectin-immunoreactive debris is observed in the outer nuclear layer, suggesting that the RPD have pierced the outer limiting membrane. Figure 4C shows a 4-dimensional rendered image of an RPD showing the relationship between the deposit and photoreceptor outer segments (green). A 3-dimensional animation is provided in Video 1 (available at www.aaojournal.org).

To confirm that RPD had an effect on photoreceptor integrity, we quantified the thickness of the ONL in regions that contained RPD compared with adjacent regions that were free of RPD. This was achieved by quantifying the thickness of the ONL in areas coincident with vitronectin staining in the subretinal space, compared with the thickness in regions devoid of vitronectin immunolabeling. As shown in Figure 4D, the ONL is significantly thinner in regions where vitronectin-immunolabeled debris is present in the subretinal space, compared with areas immediately adjacent that are devoid of immunostaining ($P < 0.05$, unpaired t test). We then correlated the area of the vitronectin immunolabeling with the thickness of the ONL to determine whether larger RPD have a greater impact on photoreceptor integrity than smaller RPD. As shown in Figure 4E, there was a positive correlation between ONL thinning and increasing RPD area (Pearson correlation, $r^2 = 0.1628$; $P < 0.05$). We also examined whether RPD were associated with cell death by examining TUNEL labeling across retinal sections that contained RPD. No TUNEL labeling of photoreceptor nuclei was noted, whereas a positive control contained many positive nuclei (an *rd1* mouse model of retinal degeneration at postnatal day 14 is known to have a high number of TUNEL-labeled photoreceptor nuclei data not shown).[21] These results suggest that RPD affect the integrity of overlying photoreceptors, but that any cell death that occurs is slow.

Retinal Stress in Regions Associated with Reticular Pseudodrusen

In view of the impact that RPD have on photoreceptor integrity, we evaluated the influence of RPD on localized retinal stress. Under normal circumstances, Müller cells of nonhuman mammalian retinae only weakly express the intermediate filament GFAP[19,22] (see patient 2 in Fig 5A). When the retina experiences stress, GFAP expression increases in Müller cells.[19,23] Similarly, in diseased conditions, Müller cells in human retina are known to increase GFAP expression.[24,25] As shown in Figure 5B, there was localized upregulation of GFAP immunoreactivity in Müller cell processes in regions adjacent to RPDs, but little GFAP immunolabeling of Müller cells in regions of the retina where RPD were absent, nor in the retina of patient 2. This observation was confirmed by quantifying the pixel intensity of GFAP immunolabeling in Müller cells within the inner plexiform layer in regions containing RPD compared with adjacent regions that were free of RPD ($P < 0.05$, unpaired t test; Fig 5D). In addition, we correlated the area of RPD (as measured by vitronectin labeling) with pixel intensity of GFAP labeling. There was no significant correlation between area of RPD and GFAP immunolabeling. These results suggest that RPD are associated with retinal stress as measured by GFAP immunolabeling, but that there is no exacerbation of gliosis in larger compared with smaller RPD.

Composition of Reticular Pseudodrusen

Conventional drusen are known to contain a large range of protein, lipid, and other moieties.[26] However, little is known about the composition of RPD. Oil Red O has been used previously to identify lipid constituents of conventional drusen[27,28] and was used here as a way of determining whether there were differences in lipid composition between RPD and conventional drusen. As shown in Figure 6A, Oil Red O−labeled deposits were located between the RPE and Bruch's membrane (conventional small drusen), but not subretinal deposits. This suggests that if there is any lipid in RPD, then the lipid composition of RPD is distinct from conventional drusen.

We examined whether immune cells were associated with RPD. Iba1 is a known marker of retinal microglia and macrophages. The subretinal deposit contained DAPI-positive nuclei, suggesting that cells are a constituent of RPD (Fig 6B, C, C′). Moreover, double labeling revealed that the cells within RPD are immunoreactive for the mononuclear cell marker Iba1. This suggests that immune cells, either microglia or macrophages, are associated with RPD. We evaluated immunolabeling of RPD for photoreceptor proteins and other proteins known to be found in conventional drusen. Deposits within RPD were immunolabeled for cone opsin as

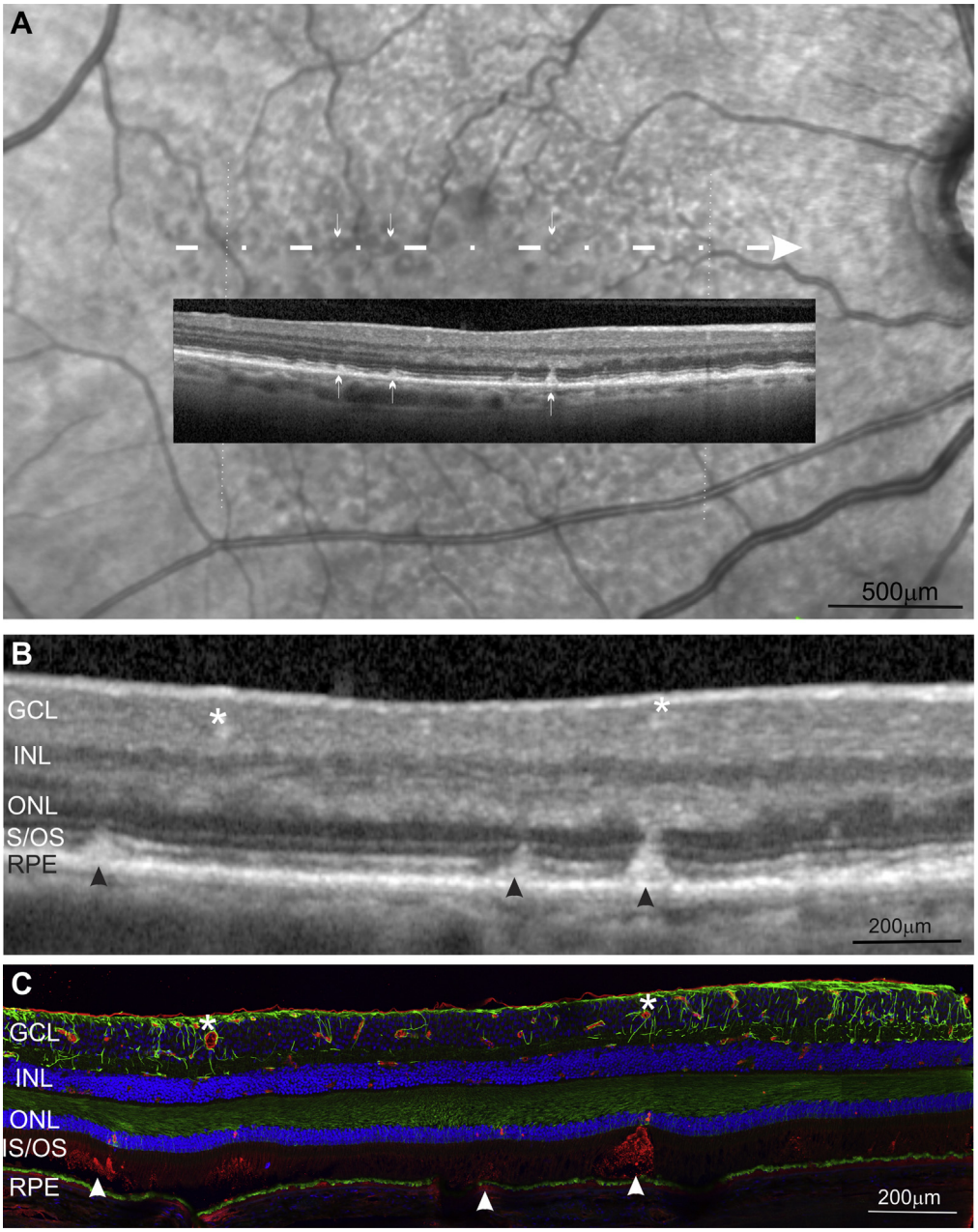

Figure 2. Coincidence of imaging and histologic results. **A**, High magnification of a red-free fundus image with optical coherence tomography (OCT) image from the central fovea of patient 1 (center inset). Several reticular pseudodrusen (RPD) are indicated by the *white arrows*. **B**, Higher magnification of the OCT image obtained from the region in (**A**) indicated by the *dotted line*. Three RPD are indicated by *black arrowheads*. Blood vessels are indicated by *asterisks*. **C**, The corresponding vertical section of retina immunolabeled with vitronectin (*red*), glial fibrillary acidic protein (*green*), and the nuclear stain DAPI (*blue*). The 3 RPD from (**B**) are shown by *white arrowheads*. GCL = ganglion cell layer; INL = inner nuclear layer; IS/OS = inner segment–outer segment junction line; ONL = outer nuclear layer; RPE = retinal pigment epithelium.

well as the glycoprotein vitronectin. In particular, vitronectin was a prominent marker of RPD and labeled all RPD, regardless of size, across the retina (Figs 3 and 6). Notably, vitronectin-immunoreactive deposits varied from large, wedge-like structures that extended into the ONL to small, flat lesions located between the photoreceptor outer segments and RPE. We also performed immunolabeling for β-amyloid as well as a range of complement factors and immune markers, including C3, C5a, CD11β, and CD102, but for these markers, no labeling was detected in human retinae from either patient, whereas control retina (mouse vertical sections) showed positive results.

Association of Reticular Pseudodrusen with Retinal Pigment Epithelium and Choroidal Changes

The cause of RPD remains controversial. Two theories for the generation of RPD have been postulated, including loss of the

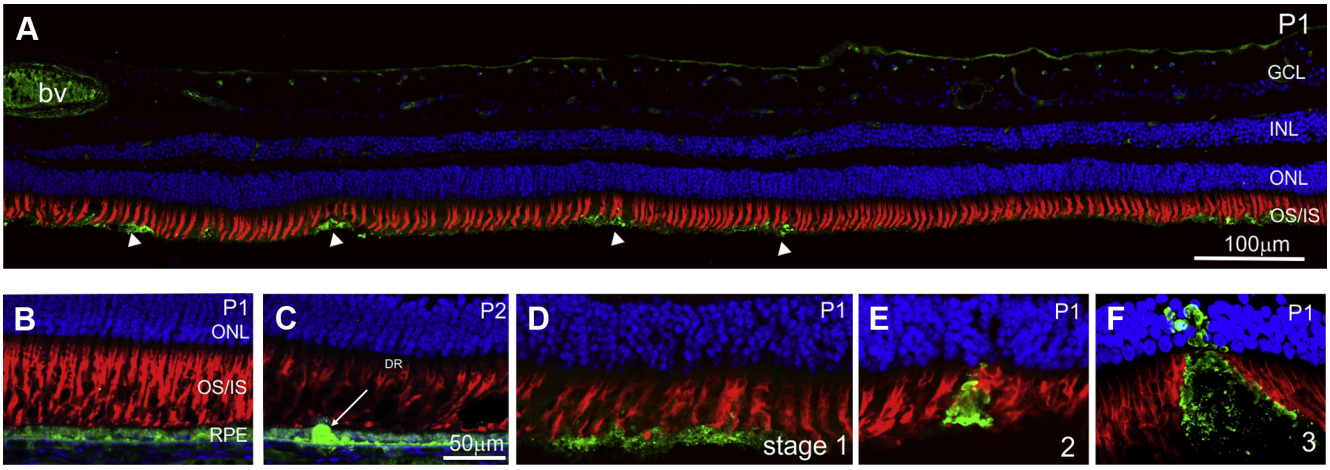

Figure 3. Different stages of reticular pseudodrusen (RPD). Vertical sections of the retina from patient 1 (P1) and patient 2 (P2) immunolabeled with vitronectin (*green*), peanut agglutinin (*red*), and a nuclear marker DAPI (*blue*). **A**, Low magnification of a section from the inferior macula of P1 showing multiple vitronectin-positive subretinal deposits (*white arrowheads*). **B**, **C**, Vertical section of the retinal pigment epithelium (RPE) and photoreceptor outer segments of (**B**) an unaffected area and (**C**) a region containing conventional drusen. Vitronectin intensely labels conventional drusen as well as basal laminar deposits. **D**–**F**, Vertical sections of photoreceptor outer segments and RPE from P1 showing different grades of RPD: (**D**) stage 1, (**E**) stage 2, and (**F**) stage 3. bv = blood vessel; GCL = ganglion cell layer; INL = inner nuclear layer; ONL = outer nuclear layer; OS/IS = outer segment–inner segment junction line.

middle vascular layer within the choroid and RPE dysfunction. We examined the choroidal vasculature from both patients and also evaluated the presence of vascular endothelium in regions immediately beneath RPD in patient 1. Notably, the vasculature was associated with endothelial cells in both patients, and there was no evidence of sclerosed choroidal vessels in regions immediately beneath RPD, suggesting that choroidal vessels remain patent across the choroid despite the presence of RPD. Notably, there appeared to be no differences in the structure of the choroid in either patient.

Retinal pigment epithelium dysfunction has been suggested as a possible contributor for debris buildup within the subretinal space. As shown in Figure 7, vitronectin-immunoreactive RPD often were associated with regions where RPE cells had migrated into the subretinal space. Anomalies in RPE cells also were visible at a higher magnification in toluidine blue–stained semithin sections (Fig 7B). Using the presence of pigment, lipofuscin, or both as a way of identifying RPE cells, we were able to confirm that Iba1-immunoreactive cells were present in most RPDs, and migrating RPE cells were located in areas adjacent, but not within, RPD. In particular, no pigmented cells were noted within RPD (Fig 6A). Phalloidin is a marker of actin filaments and labels the cellular boundaries of RPE cells. In regions where RPD were located, there was considerable irregularity in RPE cell size and shape, whereas in regions devoid of RPD, the hexagonal cell shape was more uniform. In some areas, enlarged RPE cells also were seen (Fig 7D, insert), which could be explained by the loss of RPE cells and a hypertrophy of neighboring cells in areas where RPD are located.

Discussion

The main findings of this study were that RPD were located on the subretinal side of the RPE, extending up into the outer segment layer and through into the ONL, and were associated with reduced photoreceptor integrity. In addition, the RPE in areas affected by RPD were altered compared with nonaffected areas of the RPE.

The results of this study demonstrate that RPD form characteristic lesions of varying sizes within the subretinal space that correspond to vitronectin-rich extracellular deposits. These results confirm a number of imaging studies that have suggested that RPD represent the accumulation of hyperreflective material within the subretinal space.[20,29] However, of the 3 types of RPD described by Suzuki et al,[7] the results of this study reflect the cellular detail of the most common dot form of RPD. Additional work is needed to identify whether ribbon or mid-peripheral RPD have similar characteristics to the dot type.

The results of this study show that photoreceptors are affected by the presence of RPD. In particular, the ONL was thinner in regions where RPD were located compared with neighboring RPD-free areas, and photoreceptors were pushed to the side in regions immediately overlying RPD. Our results are in agreement with those of a previous study that used adaptive optics to show a reduction in cone density overlying RPD compared with regions between the RPD.[30] In agreement with the effects on photoreceptor integrity, RPD were associated with localized Müller cell gliosis, an indicator of localized retinal stress.[19,23]

The composition of RPD remains to be defined clearly. A previous study suggested that subretinal drusenoid deposits and conventional drusen share many similarities in composition, including unesterified cholesterol, vitronectin, and complement factors, including complement factor H.[11,26] In contrast, subretinal drusenoid deposits did not label for photoreceptor-associated proteins in that study. Using immunocytochemical labeling, we found that RPD were associated with immune cells, Iba1-immunoreactive

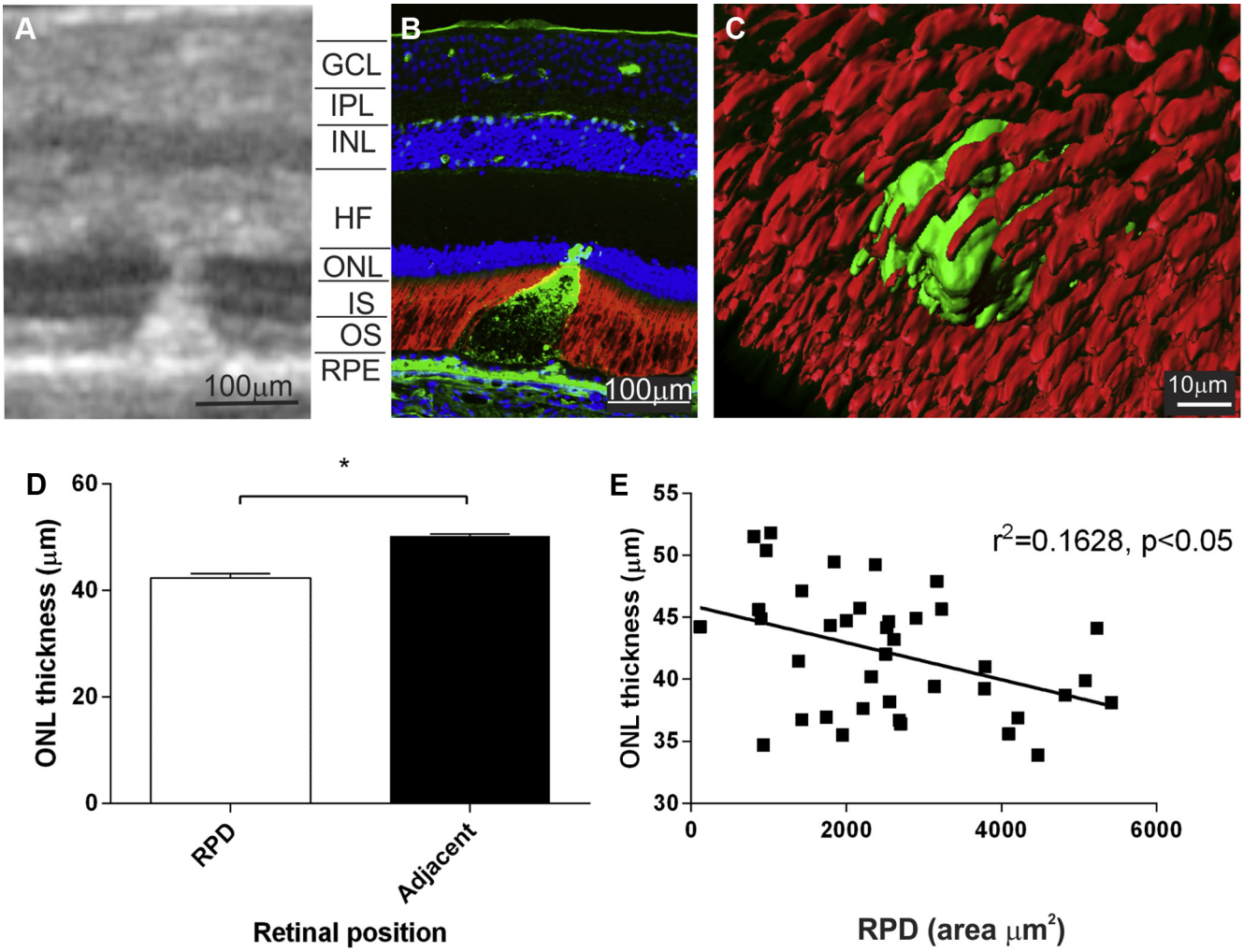

Figure 4. High magnification of reticular pseudodrusen (RPD). **A**, Optical coherence tomography image of an RPD in patient 1. **B**, Corresponding vertical section of the same RPD immunolabeled for vitronectin (*green*), peanut agglutinin (*red*), and nuclear stain DAPI (*blue*). **C**, Three-dimensional image of an RPD in the subretinal space. A deposit is visible between the outer segments of the cones. **D**, **E**, Changes in thickness of the outer nuclear layer (ONL) with RPD. **D**, Graph showing the mean plus standard error of the mean ONL thickness in regions overlying RPD and adjacent nonaffected areas. Regions without RPD showed a statistically significantly thicker ONL ($P < 0.05$). **E**, Correlation between ONL thickness and RPD area. GCL = ganglion cell layer; HF = Henle Fiber layer; INL = inner nuclear layer; IPL = inner plexiform layer; IS = inner segment; OS = outer segment; RPE = retinal pigment epithelium.

microglia and macrophages, as well as photoreceptor pigments, including opsins and peanut agglutinin. In addition, vitronectin, a plasma protein, was a prominent feature of RPD. In contrast to conventional drusen, the lipid stain Oil Red O failed to label RPD, suggesting that lipid composition is distinct between the 2 types of drusen. The differences in this and the previous study could be explained by the fixation protocols and postmortem time, which influence the intensity of immunolabeling. Alternatively, there may be subtle variations in the composition of different types of extracellular deposits or among different patients.

Our results highlight that the RPE is affected in areas where RPD are located. The RPE is known to play a critical role in maintaining the integrity of photoreceptors, playing a crucial role in outer segment phagocytosis and the recycling of retinoids.[31] It is possible that localized dysfunction or loss of RPE cells could lead to the observed accumulation of photoreceptor outer segment debris in discrete areas. Indeed, loss of RPE cells in a transgenic mouse model of conditional RPE loss was associated with localized accumulation of debris within the subretinal space as well as migration of individual RPE cells into the retina.[32] In addition, mutations in mer Tyrosine kinase, which is known to be vital for outer segment phagocytosis by RPE, are associated with photoreceptor debris accumulation in a similar location around photoreceptor outer segments and subsequent photoreceptor degeneration in rodent models of inherited retinal degeneration.[21]

There are several limitations of this study. Notably, only 1 eye from a patient with RPD was analyzed in this study. However, the fixation was rapid, occurring immediately after exenteration, minimizing any tissue effects that can

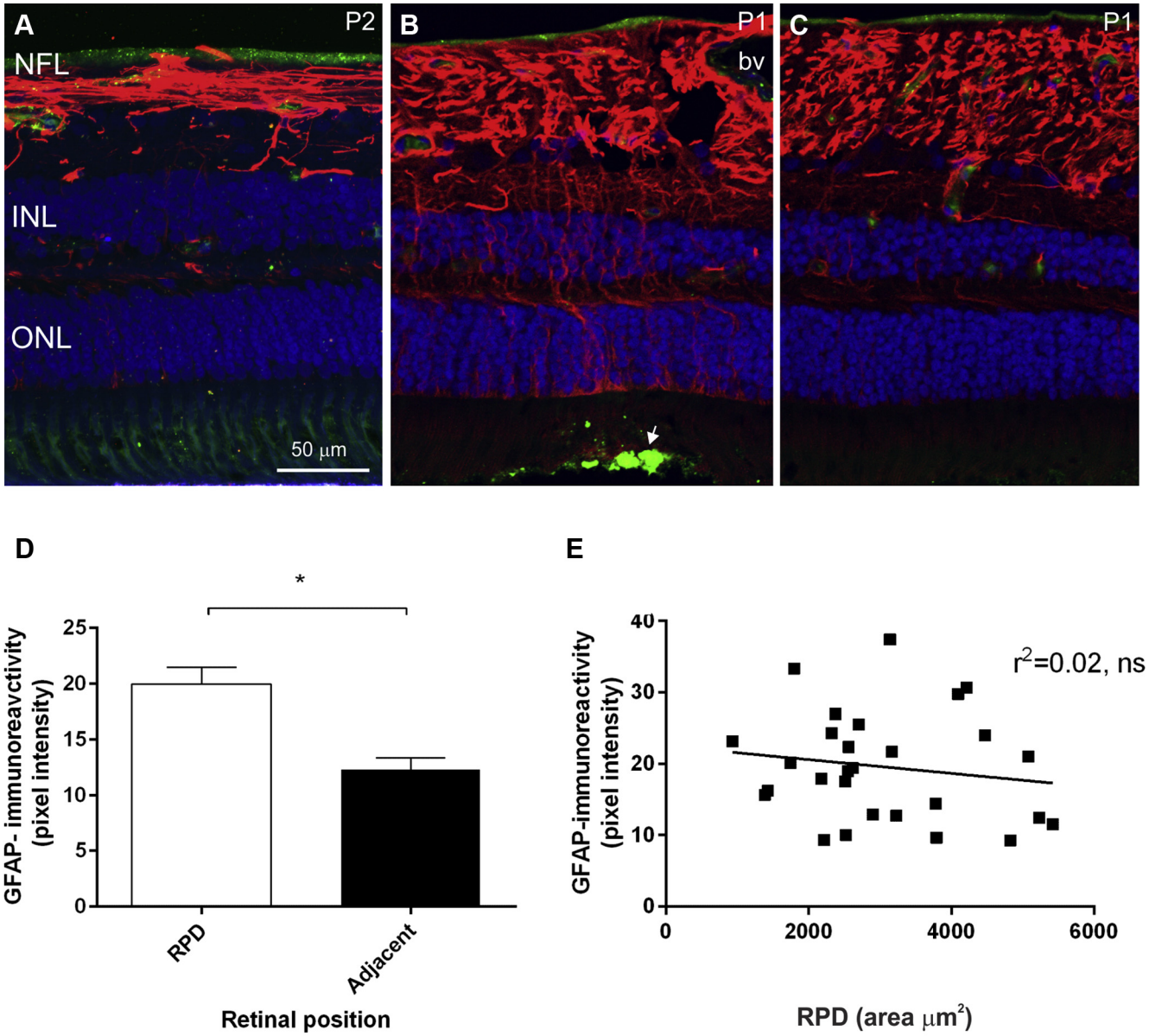

Figure 5. Localized gliosis and reticular pseudodrusen (RPD). **A**, Vertical section of retina immunolabeled for glial fibrillary acidic protein (GFAP; *red*) and vitronectin (*green*). In patient 2 (P2), GFAP labeling is concentrated at the nerve fiber layer (NFL) of the retina. **B**, **C**, Increased GFAP labeling is observed (**B**) in the region below a vitronectin-positive RPD in patient 1 (P1; *small arrow*), but (**C**) not outside the area. **D**, Graph showing the mean plus standard error of the mean GFAP pixel intensity in regions overlying RPD and adjacent nonaffected areas. Regions without RPD showed a statistically significant lower GFAP staining intensity ($P < 0.02$). **E**, Correlation between GFAP pixel intensity and RPD area. bv = blood vessel; INL = inner nuclear layer; ONL = outer nuclear layer.

occur because of postmortem time and that may have limited interpretation of previous histopathologic studies. The composition of the RPD was performed by immunocytochemical analysis. Our patient had virtually no typical drusen, whereas most eyes with RPD seen in a clinic setting have conventional drusen as well. The lack of drusen may provide a more distinct RPD phenotype than that which would be seen in the presence of multiple drusen, and as such our findings may be typical only of RPD without the presence of drusen. A far more complete list of RPD constituents is possible with unbiased gene or proteomic methods.[33] More work with more samples is required to establish the composition of RPD.

In conclusion, using human retinae that had been fixed immediately after exenteration, we established that RPD are subretinal deposits, extending into the outer segment and inner nuclear layer. Reticular pseudodrusen are associated with localized photoreceptor disruption and retinal stress. In addition, our results show that the RPE is abnormal in regions of the retina with RPD. These results highlight that RPD are a distinct type of deposit compared with conventional drusen and may be associated with RPE dysfunction.

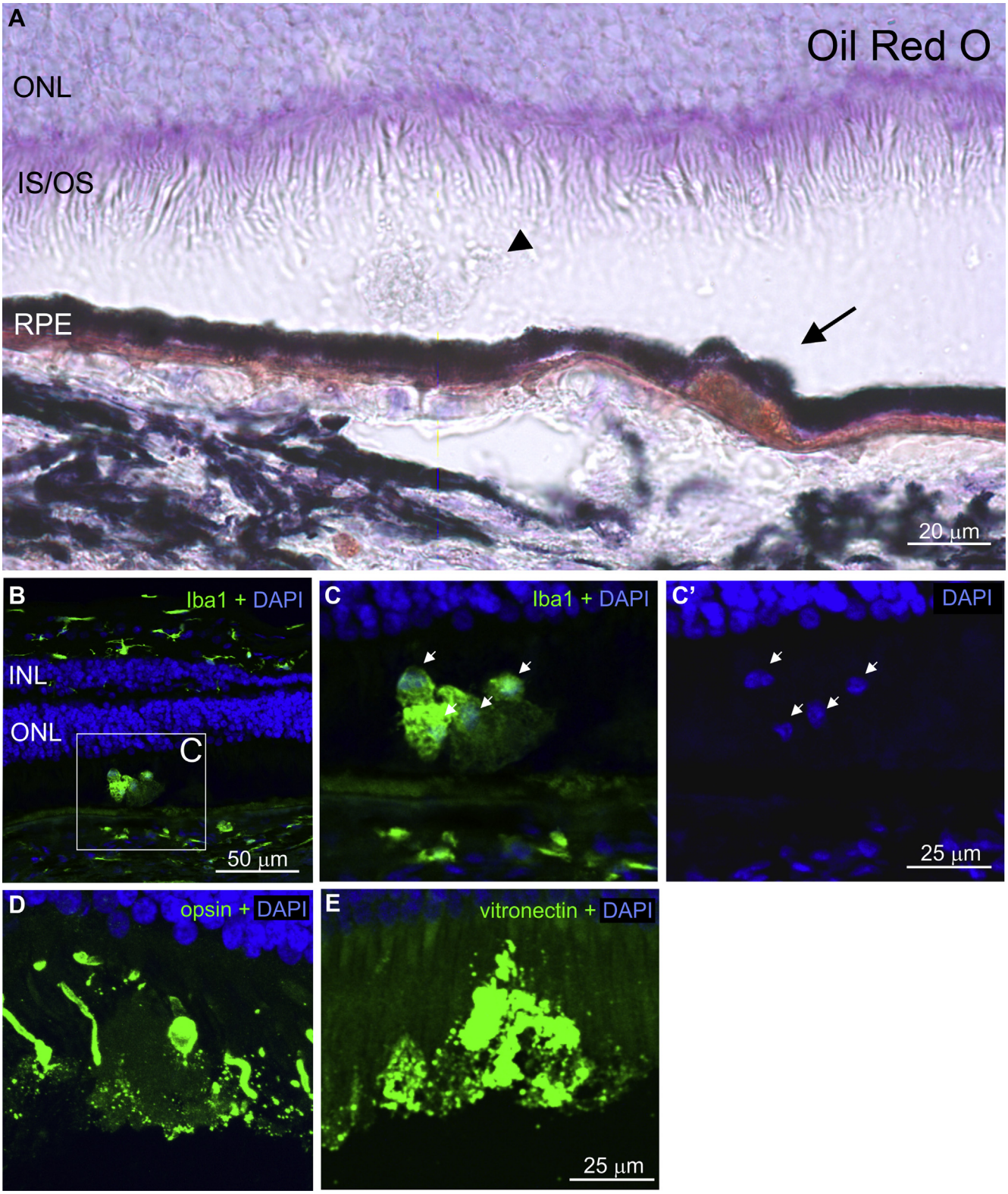

Figure 6. Composition of reticular pseudodrusen (RPD). **A**, Region of distal retina–retinal pigment epithelium (RPE) from patient 1 labeled with Oil Red O. A conventional drusen indicated by the *black arrow* is labeled. In contrast, an RPD in close proximity (*arrowhead*) is unlabeled by Oil Red O. **B**–**C′**, Vertical section through an RPD immunolabeled for IbA1 (*green*) and DAPI (*blue*) showing IbA1-positive microglia and macrophages (*arrows*). **D**, Reticular pseudodrusen immunolabeled for a combination of S and L/M cone opsins (*green*) and DAPI (*blue*). **E**, Reticular pseudodrusen immunolabeled for vitronectin (*green*) and DAPI (*blue*). INL = inner nuclear layer; IS/OS = inner segment–outer segment junction line; ONL = outer nuclear layer.

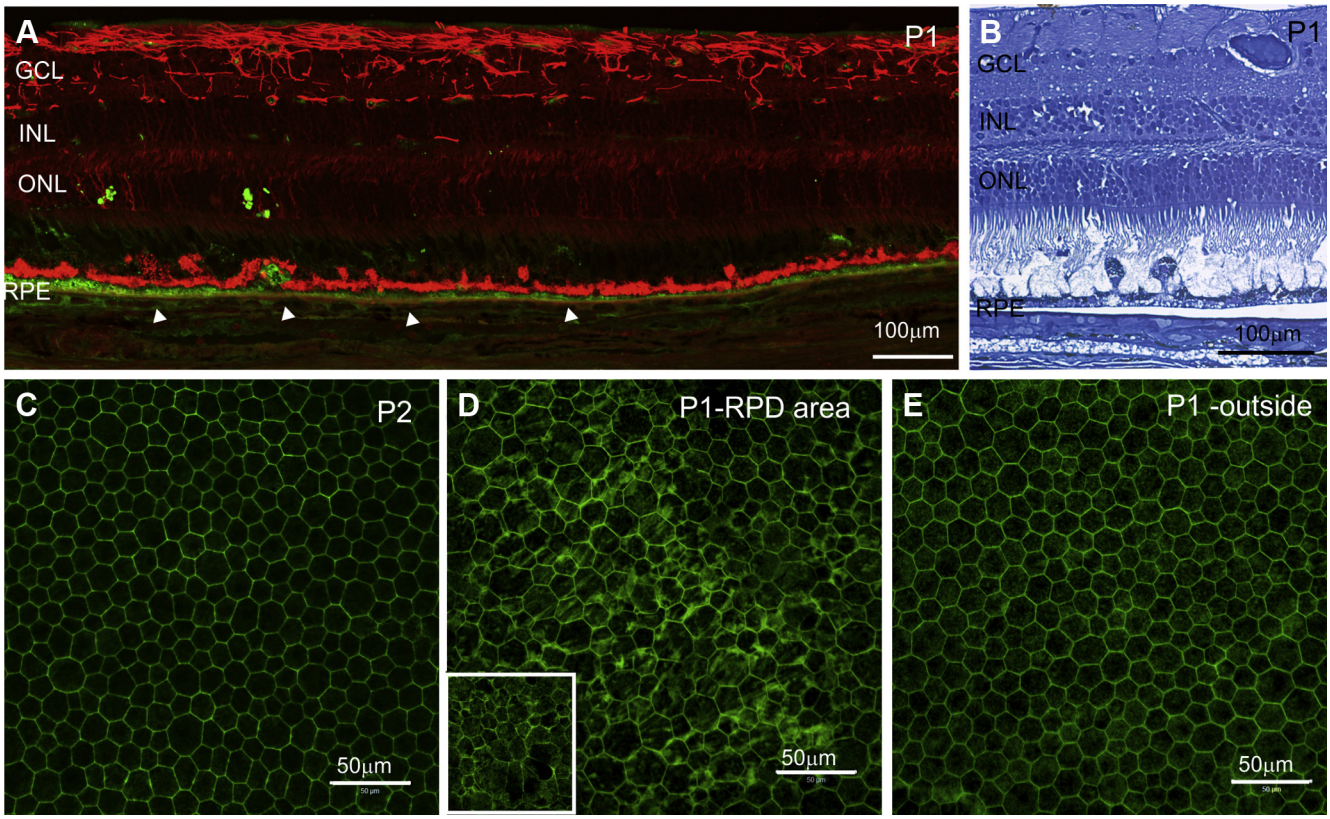

Figure 7. Anomalies in retinal pigment epithelium (RPE) and reticular pseudodrusen (RPD). **A**, Vertical section through an RPD region of patient 1 (P1) stained for glial fibrillary acidic protein (*red*) and vitronectin (*green*). Some autofluorescent RPE aberrantly invade the outer segment area of the photoreceptors (*arrowheads*). **B**, Semithin section through an RPD region of P1 stained with toluidine blue showing RPE cells aberrantly displaced toward the retina. **C**–**E**, Flat mounts of RPE stained for phalloidin (*green*) labeling the cellular boundaries of RPE cells: (**C**) flat mount of patient 2 (P2), (**D**) RPD area of P1, (**E**) outside of RPD area in P1. In regions where RPD are located, there is considerable irregularity in RPE cell size and shape, whereas in regions devoid of RPD, the hexagonal cell shape was more uniform. GCL = ganglion cell layer; INL = inner nuclear layer; ONL = outer nuclear layer.

Further work is necessary to understand more clearly the cause of RPD and their association with late AMD.

Acknowledgments. The authors thank Gene Venables for excellent technical assistance and Gavan Mitchell for help with photographic work.

References

1. Ferris FL 3rd, Wilkinson CP, Bird A, et al. Clinical classification of age-related macular degeneration. Ophthalmology 2013;120:844–51.
2. Mimoun G, Soubrane G, Coscas G. [Macular drusen]. J Fr Ophtalmol 1990;13:511–30.
3. Arnold JJ, Sarks SH, Killingsworth MC, et al. Reticular pseudodrusen. A risk factor in age-related maculopathy. Retina 1995;15:183–91.
4. Pumariega NM, Smith RT, Sohrab MA, et al. A prospective study of reticular macular disease. Ophthalmology 2011;118:1619–25.
5. Finger RP, Wu Z, Luu CD, et al. Reticular pseudodrusen: a risk factor for geographic atrophy in fellow eyes of individuals with unilateral choroidal neovascularization. Ophthalmology 2014;121:1252–6.
6. Hogg RE, Silva R, Staurenghi G, et al. Clinical characteristics of reticular pseudodrusen in the fellow eye of patients with unilateral neovascular age-related macular degeneration. Ophthalmology 2014;121:1748–55.
7. Suzuki M, Sato T, Spaide RF. Pseudodrusen subtypes as delineated by multimodal imaging of the fundus. Am J Ophthalmol 2014;157:1005–12.
8. Alten F, Clemens CR, Heiduschka P, et al. Localized reticular pseudodrusen and their topographic relation to choroidal watershed zones and changes in choroidal volumes. Invest Ophthalmol Vis Sci 2013;54:3250–7.
9. Querques G, Querques L, Forte R, et al. Choroidal changes associated with reticular pseudodrusen. Invest Ophthalmol Vis Sci 2012;53:1258–63.
10. Ueda-Arakawa N, Ooto S, Ellabban AA, et al. Macular choroidal thickness and volume of eyes with reticular pseudodrusen using swept-source optical coherence tomography. Am J Ophthalmol 2014;157:994–1004.
11. Curcio CA, Messinger JD, Sloan KR, et al. Subretinal drusenoid deposits in non-neovascular age-related macular degeneration: morphology, prevalence, topography, and biogenesis model. Retina 2013;33:265–76.

12. Spaide RF, Curcio CA. Drusen characterization with multimodal imaging. Retina 2010;30:1441–54.
13. Alten F, Eter N. Current knowledge on reticular pseudodrusen in age-related macular degeneration. Br J Ophthalmol 2015;99:717–22.
14. Sarks J, Arnold J, Ho IV, et al. Evolution of reticular pseudodrusen. Br J Ophthalmol 2011;95:979–85.
15. Jobling AI, Guymer RH, Vessey KA, et al. Nanosecond laser therapy reverses pathologic and molecular changes in age-related macular degeneration without retinal damage. FASEB J 2015;29:696–710.
16. Fritsche LG, Chen W, Schu M, et al. Seven new loci associated with age-related macular degeneration. Nat Genet 2013;45:433–9. 439e1−2.
17. Greferath U, Vessey KA, Jobling AI, et al. The role of histamine in the retina: studies on the Hdc knockout mouse. PLoS One 2014;9:e116025.
18. Downie LE, Hatzopoulos KM, Pianta MJ, et al. Angiotensin type-1 receptor inhibition is neuroprotective to amacrine cells in a rat model of retinopathy of prematurity. J Comp Neurol 2010;518:41–63.
19. Vessey KA, Wilkinson-Berka JL, Fletcher EL. Characterization of retinal function and glial cell response in a mouse model of oxygen-induced retinopathy. J Comp Neurol 2011;519:506–27.
20. Zweifel SA, Spaide RF, Curcio CA, et al. Reticular pseudodrusen are subretinal drusenoid deposits. Ophthalmology 2010;117:303–312 e1.
21. Fletcher EL, Jobling AI, Vessey KA, et al. Animal models of retinal disease. Prog Mol Biol Transl Sci 2011;100:211–86.
22. Bringmann A, Pannicke T, Grosche J, et al. Muller cells in the healthy and diseased retina. Prog Retin Eye Res 2006;25:397–424.
23. Ly A, Yee P, Vessey KA, et al. Early inner retinal astrocyte dysfunction during diabetes and development of hypoxia, retinal stress, and neuronal functional loss. Invest Ophthalmol Vis Sci 2011;52:9316–26.
24. Mizutani M, Gerhardinger C, Lorenzi M. Muller cell changes in human diabetic retinopathy. Diabetes 1998;47:445–9.
25. Wu KH, Madigan MC, Billson FA, et al. Differential expression of GFAP in early v late AMD: a quantitative analysis. Br J Ophthalmol 2003;87:1159–66.
26. Rudolf M, Malek G, Messinger JD, et al. Sub-retinal drusenoid deposits in human retina: organization and composition. Exp Eye Res 2008;87:402–8.
27. Curcio CA, Johnson M, Huang JD, et al. Aging, age-related macular degeneration, and the response-to-retention of apolipoprotein B-containing lipoproteins. Prog Retin Eye Res 2009;28:393–422.
28. Pauleikhoff D, Harper CA, Marshall J, et al. Aging changes in Bruch's membrane. A histochemical and morphologic study. Ophthalmology 1990;97:171–8.
29. Zhang Y, Wang X, Rivero EB, et al. Photoreceptor perturbation around subretinal drusenoid deposits as revealed by adaptive optics scanning laser ophthalmoscopy. Am J Ophthalmol 2014;158:584–596 e1.
30. Mrejen S, Spaide RF. The relationship between pseudodrusen and choroidal thickness. Retina 2014;34:1560–6.
31. Strauss O. The retinal pigment epithelium in visual function. Physiol Rev 2005;85:845–81.
32. Longbottom R, Fruttiger M, Douglas RH, et al. Genetic ablation of retinal pigment epithelial cells reveals the adaptive response of the epithelium and impact on photoreceptors. Proc Natl Acad Sci U S A 2009;106:18728–33.
33. Anderson DH, Radeke MJ, Gallo NB, et al. The pivotal role of the complement system in aging and age-related macular degeneration: hypothesis re-visited. Prog Retin Eye Res 2010;29:95–112.

Footnotes and Financial Disclosures

Originally received: November 11, 2015.
Final revision: February 4, 2016.
Accepted: February 4, 2016.
Available online: March 30, 2016. Manuscript no. 2015-1999.

[1] Department of Anatomy and Neuroscience, The University of Melbourne, Parkville, Australia.

[2] Centre for Eye Research Australia, Royal Victorian Eye & Ear Hospital, East Melbourne, Australia.

[3] Departments of Ophthalmology and Surgery, University of Melbourne, Parkville, Australia.

*Both Ursula Greferath, PhD, and Robyn H. Guymer, PhD, contributed equally as first authors.

Financial Disclosure(s):
The author(s) have no proprietary or commercial interest in any materials discussed in this article.

Supported by the National Health and Medical Research Council of Australia, Canberra (grant nos.: APP1027624 and 1061419 [R.H.G., K.A.V., E.L.F.]); and the Macular Diseases Foundation of Australia Sydney (R.H.G., K.A.V., E.L.F.).

Author Contributions:

Conception and design: Guymer, Fletcher

Analysis and interpretation: Greferath, Guymer, Vessey, Fletcher

Data collection: Greferath, Guymer, Brassington, Fletcher

Obtained funding: none

Overall responsibility: Greferath, Guymer, Vessey, Brassington, Fletcher

Abbreviations and Acronyms:
AMD = age-related macular degeneration; **GFAP** = glial fibrillary acidic protein; **OCT** = optical coherence tomography; **ONL** = outer nuclear layer; **RPD** = reticular pseudodrusen; **RPE** = retinal pigment epithelium; **SD** = spectral-domain; **TUNEL** = terminal deoxynucleotidyl transferase dUTP nick end labeling.

Correspondence:
Erica L. Fletcher, PhD, Department of Anatomy and Neuroscience, The University of Melbourne, Grattan Street, Parkville 3010, Victoria, Australia. E-mail: elf@unimelb.edu.au.